The Austrian Journal of Technical and Natural Sciences, No 11–12
ISSN 2310-5607

PREMIER Publishing
ppublishing.org

DOI:10.29013/AJT-24-11.12-28-37

SYNTHESIS OF NANOCOMPOSITE MATERIALS AND THEIR PROPERTIES BASED ON POLYMETHYLENE NAPHTHYLENESULFONATE AND TiO2 NANOTUBES

Djumagulov Sh. Kh. [1], ***Khamidov A. M.*** [2], ***Todjiev J. N.*** [1], ***Nurmanov S. E.*** [1], ***Rozimuradov O. N.*** [2]

[1] National University of Uzbekistan, Uzbekistan

[2] Turin Polytechnic University in Tashkent

Cite: *Djumagulov Sh. Kh., Khamidov A. M., Todjiev J. N., Nurmanov S. E., Rozimuradov O. N. (2024). Synthesis of Nanocomposite Materials and Their Properties Based on Polymethylene Naphthylenesulfonate and TiO_2 Nanotubes Austrian Journal of Technical and Natural Sciences 2024, No 3–4.* https://doi.org/10.29013/AJT-24-11.12-28-37

Abstract

In this article, the optimal conditions for the formation of nanotubes based on titanium oxide were determined and the synthesis of nanotubes was carried out. The obtained material was studied using scanning electron microscope (SEM) and IR-spectroscopy methods. Naphthalene-based copolymer products were obtained, their formation mechanisms,^{1}H and^{13}C spectra were studied. Nanocomposite products based on titanium oxide were synthesized and volt-amperometric properties of obtained nanocomposite materials were determined.

Keywords: *anodization, pore formation kinetics, volt-amperometric properties*

Introduction

In the last decade, electrochemical synthesis and anodization process have attracted more attention (Yu, C., et al., 2019; Sun, X., et al., 2019; Zhang, K., et al., 2019). Porous anodic oxides, such as porous aluminum and titanium nanotubes, have attracted great scientific interest because their nanomaterials are used in many fields, especially anodic titanium oxide nanotubes (ATO) in solar energy conversion, supercapacitor, sensor, photocatalytic decomposition and is also of great importance in the fields of converting solar energy into hydrogen fuel (Lee, W., et al., 2014; Cheng, Y., et al., 2015; Li, Z., et al., 2018). The formation of pores and formation of nanotubes depends on such parameters as concentration of the electrolyte composition, anode voltage, current density, temperature of the electrolyte.For example, the height of nanotubes differs from each other in different literature (Feng, C., et al., 2019; Wang, K., et al., 2014; Lee, K., et al., 2014). At the same concentration of ammonium fluoride (0.3% NH_4F) and ethylene glycol electrolytes, it was reported that the height of the obtained nanotubes was significantly different from each other (Zhang, Y., et al., 2015). Zhang et al. 4.7 μm long nanotubes were obtained at a current density of 7.5 mA·cm-2, Sui et

al. reported that the height of the nanotubes obtained as a result of anodizing at a current density of 10 mA·cm-2 for 45 minutes was 15.3 μm (Cui, H., et al., 2017). Liu et al. reported that the height of the nanotubes was 8.5 μm obtained by anodizing at a constant voltage of 50 V for 60 minutes (Li, W., et al., 2019). .Masak et al. They studied the effect of Ti substrate on nanotube growth and size in 0.3% NH_4F electrolyte, nanotubes with a height of 32 ~ 50 μm were obtained by anodizing at 60 V for 360 minutes (Sopha, H., et al., 2016). It can be seen that the anodizing voltage, anodizing current, Ti substrate, and anodizing time are different in the electrolyte with the same concentration of NH_4F, resulting in a large difference in the height of the nanotubes. This means that the electrochemical dissolution reaction in the presence of fluoride ions ($TiO_2+6F^-+4H^+\rightarrow[TiF_6]_2^-+$ $+2H_2O$) is not a factor determining the nanotube height (Zhang, J., et al., 2018) synthesized nanotubes with a height of 29.8 μm in an ethylene glycol electrolyte containing 0.30% NH_4F and 2% water at 60 V for 180 minutes. Zhao et al. height of nanotubes reported that the height of nanotubes obtained by anodizing at 60 V for 10 minutes in an ethylene glycol electrolyte consisting of 0.50% NH_4F and 2% water was 9.0 μm (Zhao, S., et al., 2018). However, Liu et al. also reported that the height of nanotubes obtained by constant voltage anodization at 60V for 360 minutes in an ethylene glycol electrolyte consisting of 0.83% NH_4F and 8% water was 10 μm (Wang, L., et al., 2024).This is due to the fact that the fluoride ion participates in the melting reaction and the water content affects the height of the nanotubes.

Experimental part

A 0.1 mm thick titanium foil (99.8% purity, Sigma Aldrich) was cut into strips (10 mm × 40 mm) and polished. To clean the surface of the foil from various roughnesses and inclusions, it was cleaned in a solution consisting of HF: HNO_3: H_2O = 1:1:2) for 15 minutes (GT Sonic-D 6, AC-220–240V). Then it was washed in distilled water for another 15 minutes and air-dried for one hour. After that, an electrolyte containing 2% water, 98% ethylene glycol solution with 0.1 and 0.2% NH_4F was prepared. Titanium foil was used as the anode and graphite electrode was used as the counter electrode. A titanium foil immersed in an electrolyte has an area of 4 cm2 (2cm×1cm×2 sides). The voltages were applied in different sequence from 30V to 70 V (Potentiostat: (Model-SS-350M, S/N 21121062). Anodizing time was 2, 3, 4 and 6 hours and two electrodes were kept constant in two different electrolytes. anodizing voltages were applied and each process was repeated three times.The anodizing process was 20 °C, 50 V and The nanotubes obtained at 20 °C, 60 V showed the formation of highly ordered nanotubes with a flat surface.

Results and its discussion

Figure 1 shows the variation of electric current and formation of TiO_2 nanotubes at 20 °C 50 B, 0.1% NH_4F.

Figure 1. *20 °C 50 B, 0.1% NH_4F, electric current change and TiO_2 nanotube formation diagram (I), (II), (III)*

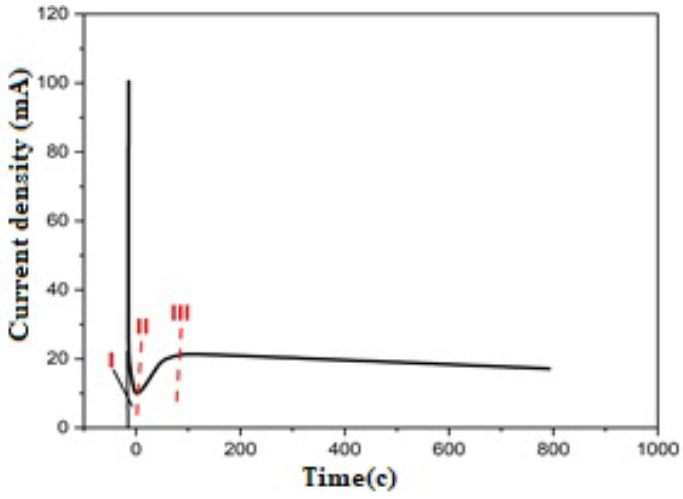

Figure 1 (20 °C 50 B, 0.1% NH_4F) shows the formation of pores in stage I initially at 100 mA, in stage II at 101 mA and 10 s, and in stage III, the nanotubes are fully formed. It can be seen that t, the time and the current are in the same state, i.e. at 20 mA, it continued in the range of 10–800. The formation of nanotubes at this anodic voltage resulted in the formation of double-walled nanotubes with a uniform flat surface and highly ordered (Figures 2a, b).

Figure 2. *SEM-EDS (a-b) of nanotubes obtained in 0.1% NH_4F at 20 °C, 50V and the resulting formation time (c)*

a)

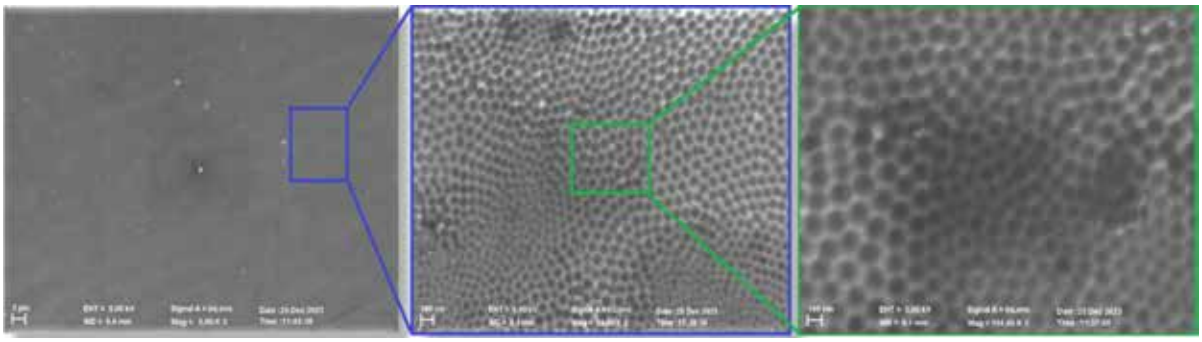

b)

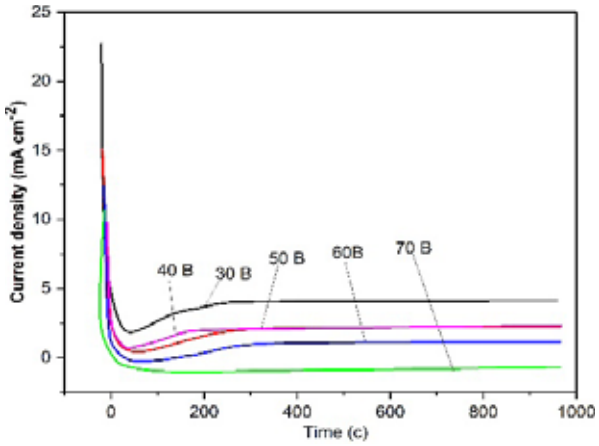

c)

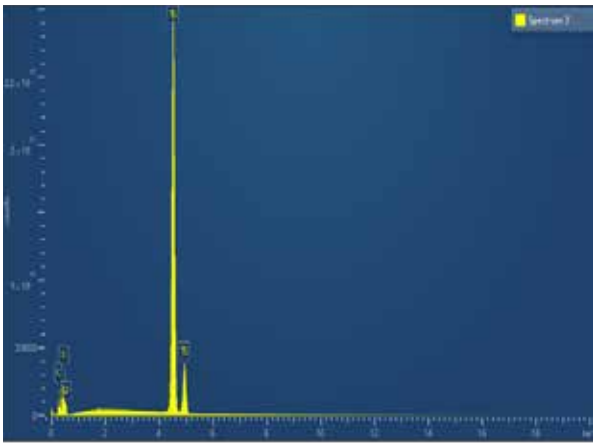

The element composition is 67.55% Ti, 30.45% O and 2% C. Looking at the time curves of the formed current at 20 °C, (30––70 V) in the presence of 0.1% NH_4F, it can be seen that initially at 30 V 22.5 mA 10 s pore formation begins, but they are not uniform. can be seen. At 40V, 9.9 mA started to form pores at 9 s, 50 V at 15mA at 8.5s, at 60 V 12.5 mA at 8 s and continued to form pores, and at 70 V at 10.8 mA starting at 7.5 s, irregular and flat it can be seen that the nanotubes formed without,

It can be concluded that the nanotubes formed at 50 V, 8.5 seconds and 60 V, 8 seconds have a flat surface and higher order than the nanotubes formed at other voltages. Formation of nanotubes As can be seen from Figures 3 a, b, double-walled nanotubes with uniform flat surface and high order were formed. The element composition is 65.55% Ti, 31.45% O and 3% C. Looking at the time curves of nanotube formation (Fig. 3 c), 30 V, 20 mA showed that disordered pores started to form in 10 s, 40 V, 7 mA showed highly disordered pores in 9.5 s, 50 V, 12 mA 9 seconds and 60V, 11mA in 8 seconds high-order flat surface, 70 V 10 mA At 7.5 seconds, you can see that nanotubes with irregular but smooth surface are formed. It can be concluded that the nanotubes formed at 50 V, 12 mA 9 seconds and 60 V, 11 mA 8 seconds, while the nanotubes formed at other voltages are known to have a smooth surface and higher order.

Figure 3. *Of nanotubes obtained in 0.2% NH_4F at 20 °C, 60 V. SEM-EDS (a-b) and formation time results (c)*

a)

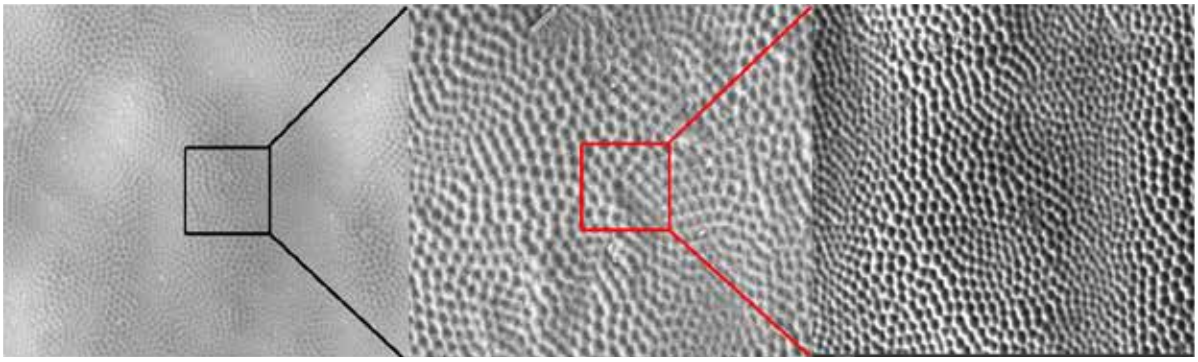

b) c)

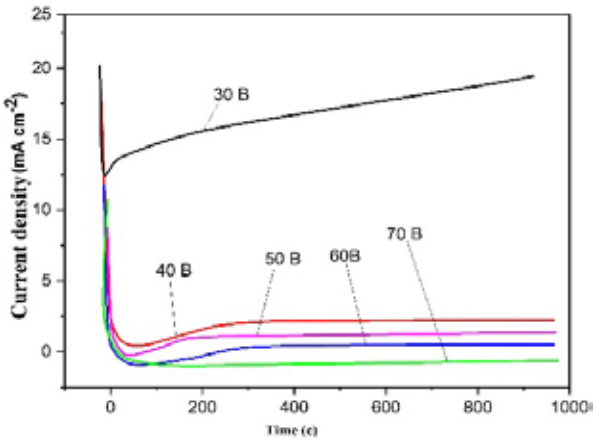

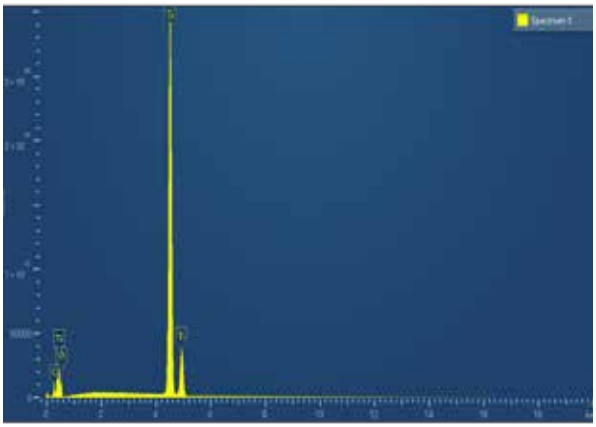

2. Synthesis of polymethylene naphthalene sulfonate (PMNS)

The process of obtaining a copolymer product consists of the following stages:

1. Sulfolation of the naphthalene fraction. 64 g of naphthalene-based fraction (210–250 °C) was placed in a three-necked flask equipped with a mechanical stirrer, a dropping funnel and a reflux condenser, heated to 140 °C and liquefied, and 3 ml/ml of 60 g of sulfuric acid solution of 98% was added using a funnel. min dripped. Since the process was exothermic, the temperature rose to 160–165 °C. In this case, the process was continued for 4 hours. The reaction equation is:

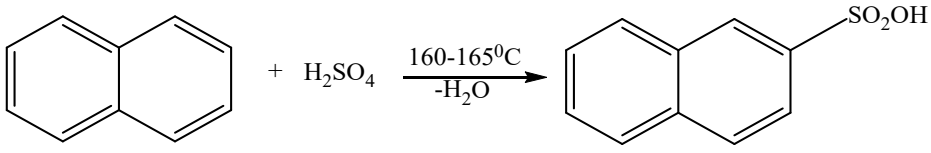

process mechanism:

$$2H_2SO_4 \rightleftharpoons H_3SO_4^+ + HSO_4^-$$

$$H_3SO_4^+ \rightleftharpoons SO_3H^+ + H_2O$$

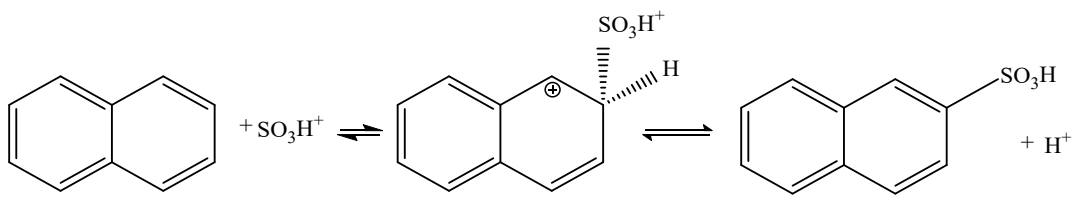

Table 1. *Conditions for the synthesis of 2-naphthalenesulfoacid*

Substance name	Mole ratio of naphthalene and H_2SO_4 (98% li).	Tempera-ture, °C	Duration of the reaction, hours	Reaction product (%)
1-Naphthalene sulfonic acid	1:1.2	60	4	48
			6	56
			8	54
	1:1.2	70	4	58
			6	69
			8	61
	1:1.2	80	4	83
			6	**91**
			8	85
	1:1.2	90	4	79
			6	84
			8	76
2-Naphthalene sulfonic acid	1:1.08	140	4	54
			6	59
			8	55
	1:1.08	150	4	67
			6	82
			8	78
	1:1.08	160	4	81
			6	**89**
			8	90
	1:1.08	170	4	71
			6	86
			8	76

Figure 4. *IR spectrum of 2-sulfonaphthalene*

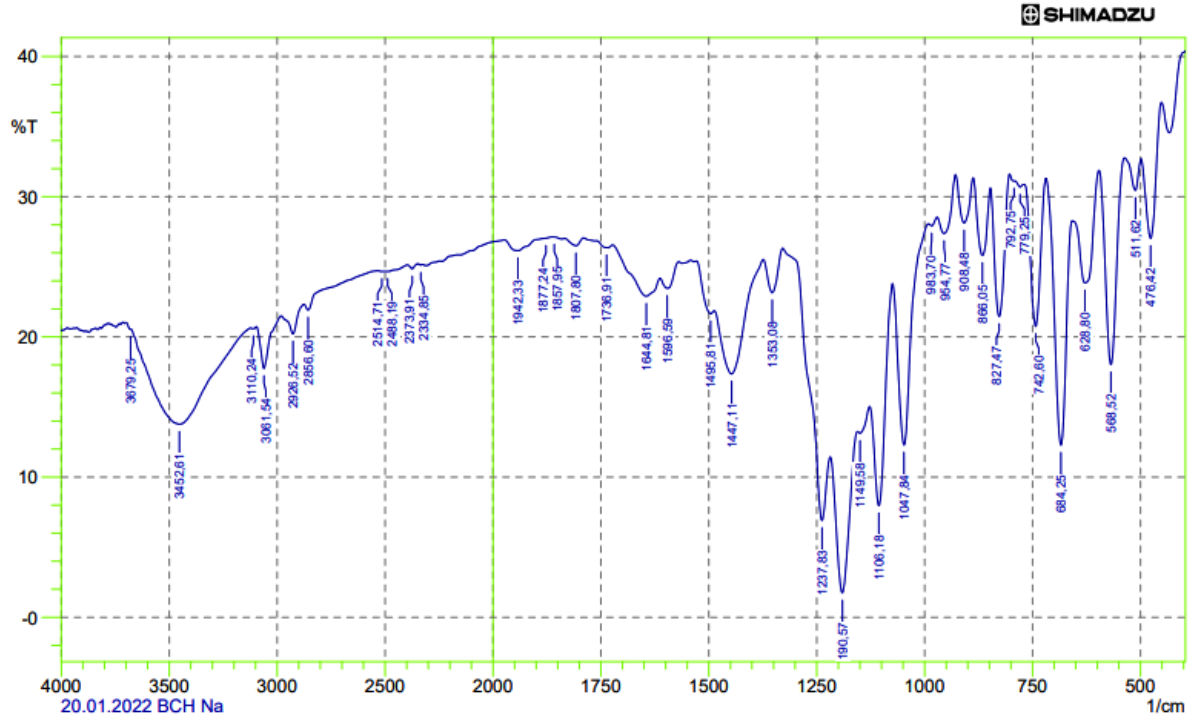

The optimal conditions for the synthesis of 2-naphthalene sulfoacid were naphthalene and sulfuric acid in the ratio of 1:1.08 mol, at a temperature of 160 °C and a process duration of 6 hours, with an efficiency of 89%. During the synthesis of 1 and 2 naphthalene sulfoacids, increasing the duration of the reaction leads to a decrease in yield. Because, as a result of additional reactions (oxidation, 1.1 and 2.2-sulfonyldinaphthalene), the yield of naphthalene sulfoacids decreases.

The vibrational frequency is the valence vibration of the -C-H group in the aromatic nucleus in the 3061.54 cm^{-1} area, the valence vibration of the C=C bond in the aromatic nucleus in the 1596.59 cm^{-1} area, the valence vibration of the aromatic nucleus in the 742.6 cm^{-1} area, the valence vibration of the -SO_3H group in the 1106.18 cm^{-1} area vibration, the valence vibration of the C=O bond can be observed in the region of 1190.57 cm^{-1}.

2. Polycondensation of β-naphthalene sulfoacid with formalin (35%). The process was carried out in a hermetic reactor equipped with a mechanical stirrer. For the reaction, *β*-naphthalene sulfonic acid and formaldehyde were taken in a ratio of 1:0.8 mol, and the process was carried out at 90–100 °C for 5 hours. As a result, polymethylenenaphthalene sulfonic acid was synthesized with a yield of 82.4% (Cheng, Y., Peng, Z., Wu, X., Cao, J., Skeldon, P., & Thompson, G. E., 2015). The polycondensation reaction scheme is as follows:

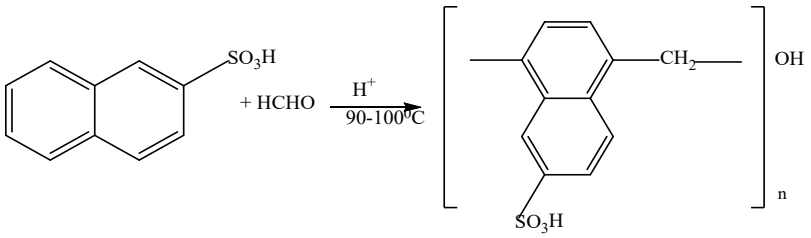

Mechanism of action:

$$H_2SO_4 + H_2O \rightleftharpoons HSO_4^- + H_3O^+ \quad \text{I.}$$

$$H_2SO_4 + H_2SO_4 \rightleftharpoons HSO_4^- + H_3SO_4^+ \quad \text{II.}$$

$$H_3SO_4^+ \rightleftharpoons H_2SO_4 + H_+ \quad \text{III.}$$

$$CH_2O + H^+ \longrightarrow {}^+CH_2OH \quad \text{IV.}$$

$$ArH + {}^+CH_2OH \longrightarrow \begin{cases} Ar\text{-}CH_2^+ + H_2O \\ Ar\text{-}CH_2\text{-}OH + H^+ \end{cases} \quad \text{V.}$$

$$Ar\text{-}CH_2^+ + Ar\text{-}H \longrightarrow Ar\text{-}CH_2\text{-}Ar + H^+ \quad \text{VI.}$$

1 H and 13 C NMR spectra of the resulting polymer

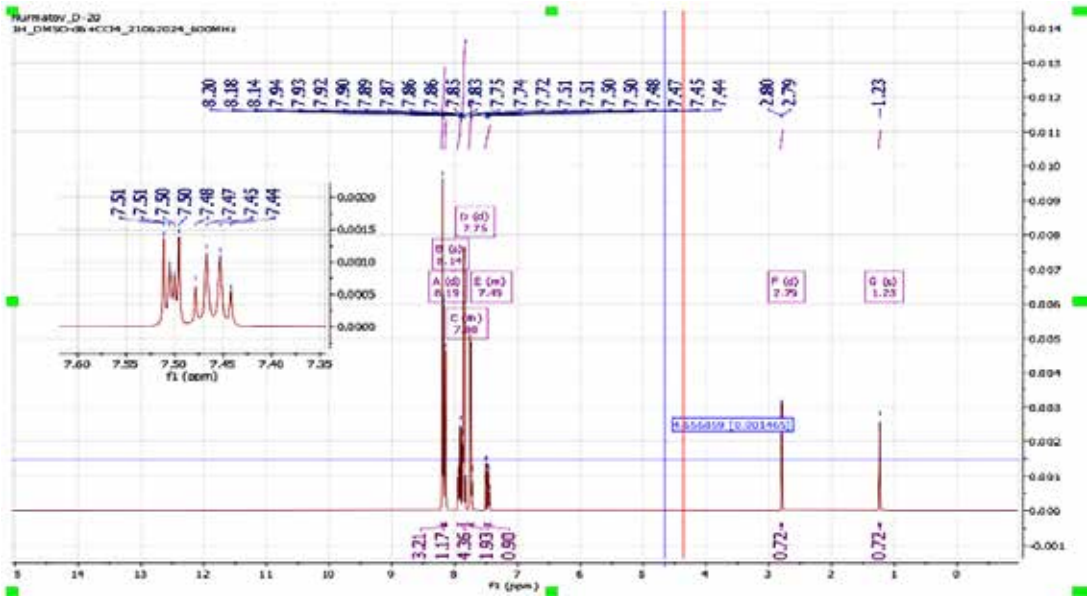

(Polymethylenenaphthalene sulfonate acid1H) YaMR (600 MHz, DMSO-D_6) δ 8.19 (d, J = 11.8 Hz, 3H), 8.14 (s, 1H), 7.95–7.81 (m, 4H), 7.75 (d, J = 0.0 Hz, 2H), 7.53–7.43 (m, 1H), 2.79 (d, J = 5.0 Hz, 1H), 1.23 (s, 1H).

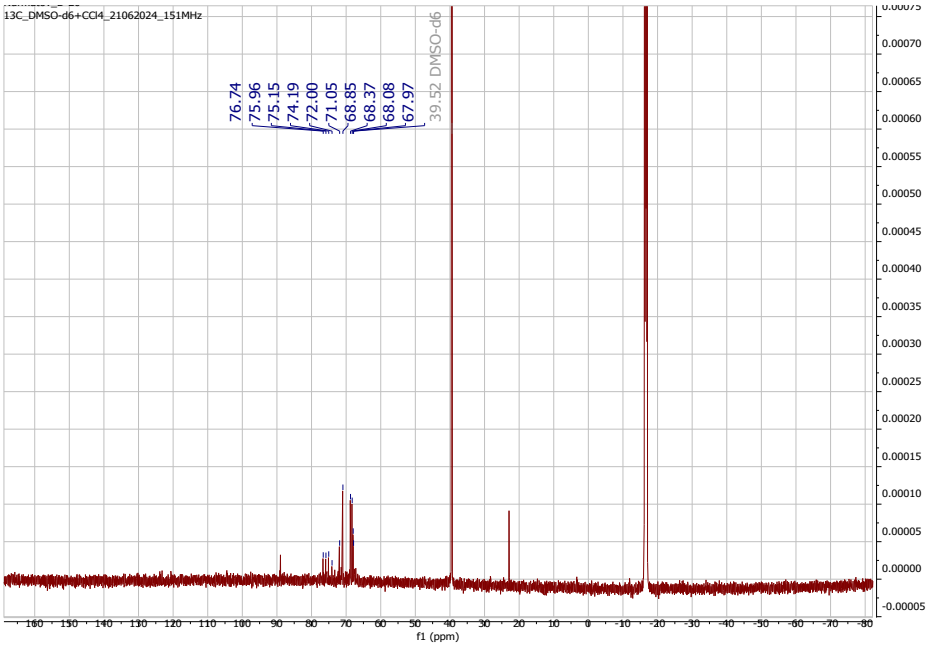

(Polymethylenenaphthalene sulfonate acid13C) YaMR (151 M Hz, DMSO-D_6) δ 76.74, 75.96, 75.15, 74.19, 72.00, 71.05, 68.85, 68.37, 68.08, 67.97.

SEM was used to determine the morphology and surface structure and elemental composition of spatially structured polymethylenenaphthalene sulfoacids (Fig. 5). The results of the SEM analysis of polymethylenenaphthalene sulfoacid are presented in pictures (c, d). The SEM result shows that it contains macropores from 114 μm to 613 μm. The composition of the element consists of 68.3% C, 18.1% O.

3. Preparation of nanocomposite materials and their physical and hemical characteristics. To carry out this experiment, the following processes were carried out: an electrochemical polymerization process, using titanium oxide nanotubes as anode and graphite as counter electrode and polymer dissolved in DMSO (15g polymer dissolved in 100 g DMSO) as electrolyte. The titanium oxide nanotubes immersed in the electrolyte have an area of 4 cm^2 (2 cm × × 1 cm × 2 sides). Voltages were made at 50 V, 60 V, respectively. Anodizing voltages were continuously applied to two electrodes in five different electrolytes for 4 hours. Each step of anodization was repeated three times.

Figure 5. *SEM-EDS analysis of polymethylene sulfonate naphthalene*

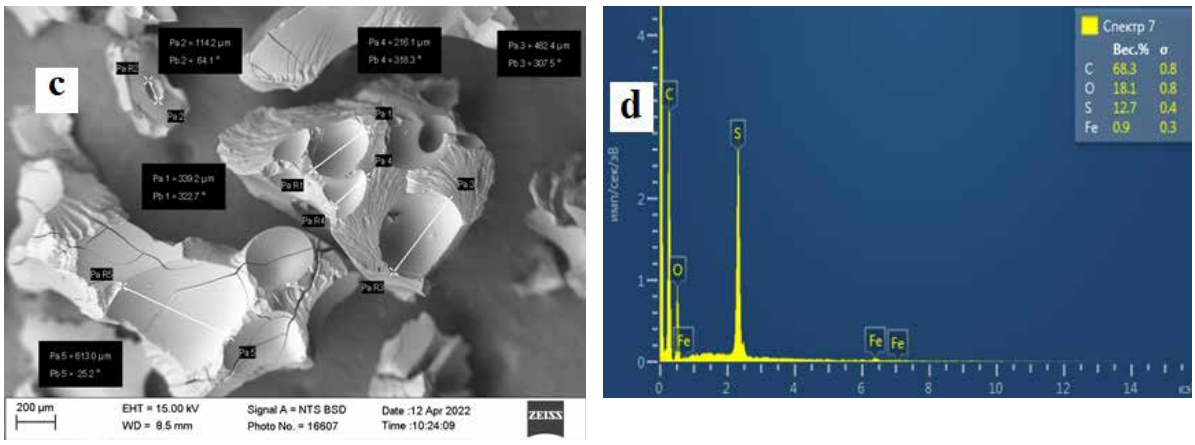

Figure 6. *SEM micrographs of nanocomposites formed on the basis of nanotubes containing 2, 10 and 45% water*

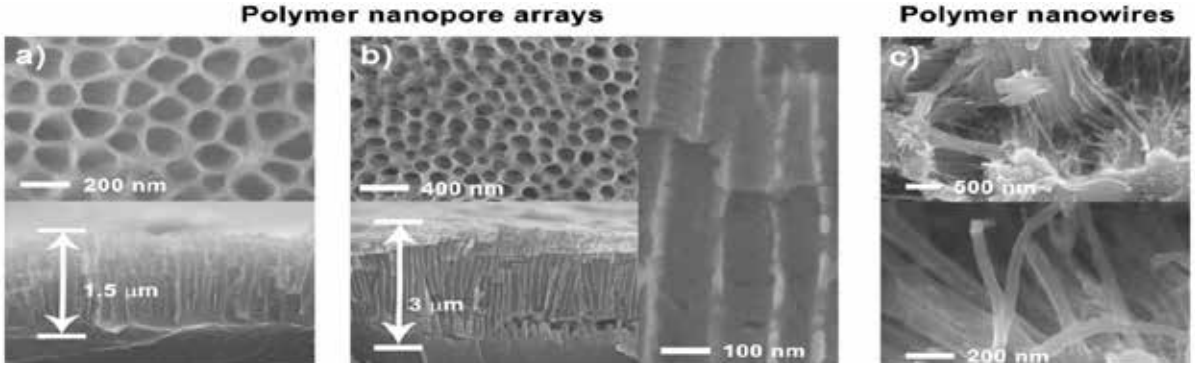

Figure 6a shows that the nanotubes with 2% water have a flat surface and are ordered with a side length of 1.5 microns, (b) the pores formed at 10% water are irregular but with a side length of 3 microns, (c) At 45% water, we can see that nanotubes are formed randomly.

Figure 7. *IR spectrum of the obtained nanocomposite*

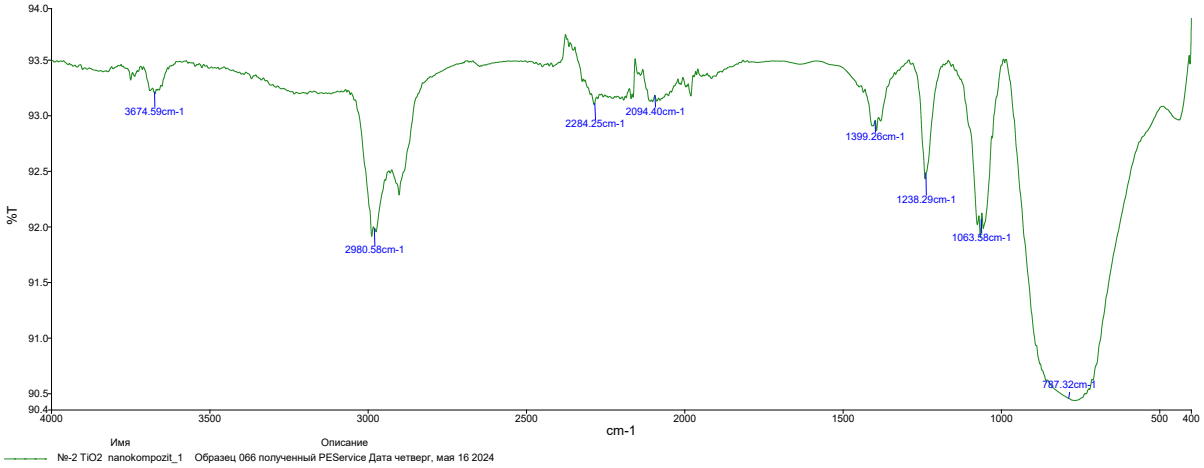

The vibrational frequency is the valence vibration of the -Ti-O bond in the aromatic nucleus in the 787.3 cm^{-1} region, the valence vibration of the C=C bond in the aromatic nucleus in the 2980.58 cm^{-1} region, the valence vibration of the -SO_3H group in the 1063.58 cm^{-1} region, and the 1238.29 cm^{-1} region In the –1 region, the valence vibration of the C=O bond can be observed.

The volt-ampere characteristics of the obtained nanocomposites (0–1.5 V) were studied:

Figure 8. *Volt-ampere characteristic of nanocomposite containing 2% H_2O*

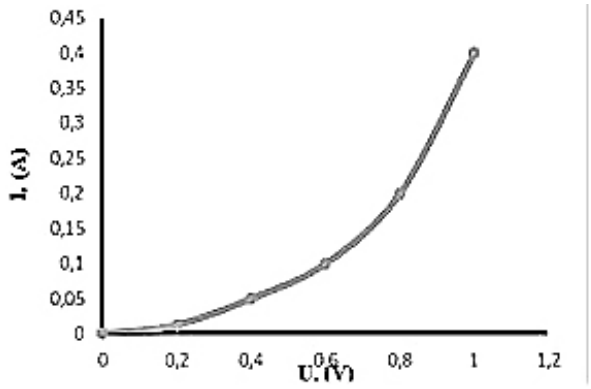

Figure 9. *Volt-ampere characteristics of forward and reverse conductivity of nanocomposite samples*

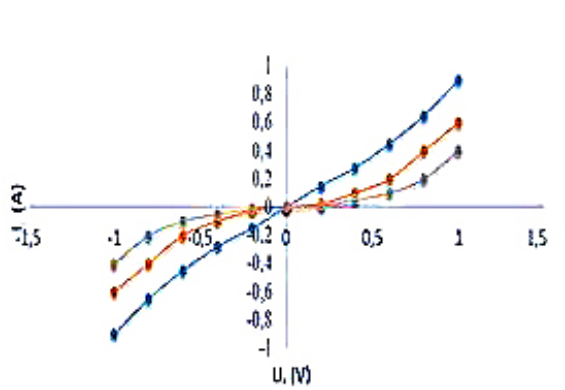

The volt-amperometric characteristics of nanocomposite materials in the range (0–1.5V) were studied. In Figure 8, the sample in 2% water in the electrolyte is initially in the ranges from 0 to 1V, that is (0.2 V–0.0125 A, 0.4 V-0.025 A, 0.6V–0.05 A, 0.8 V–0.09 A, and at 1V 0.15 A) it can be seen that the electrical conductivity of nanotubes increases. Figure 9 shows the diagram of the volt-amperometric characteristics of the samples in forward and reverse quenching (2%, 10% and 45% water in the electrolyte) it can be seen that the conductivity is good.

This table shows the relative electrical conductivity of nanocomposites obtained at different voltages (from 30 V to 70 V). We can see that the highest values are 14.500 at 50 V and 22.100 at 60 V. It is known from the table that these values are low in the remaining voltages.

Activation energies and specific electrical conductivity values of polymer composites based on TiO2 (U= 0.5 V)

№	Voltage (V)	TiO_2 E, ev	Relative electrical conductivity, Sm/sm
1.	30	0.210	13.200
2.	40	0.092	2.400
3.	50	0.090	14.500
4.	60	0.120	22.100
5.	70	0.070	0.005

Summary

The volt-ampere characteristics of the polymer obtained on the basis of naphthalene and its nanocompositions with metal oxides (TiO2), the activation energies of electrical current conductivity were determined. It was found that the electrical conductivity of polymethylene naphthalene sulfonate acid is “p” type, and its nanocompositions with metal oxides are “n” type conductive materials.

Technical conditions of storage, use and other indicators of composite materials based on polymethylenenaphthalene sulfonate have been developed. The practical importance of polymer nanocomposites can be explained by the fact that they can be used as components of electrode materials for rechargeable batteries and supercapacitors, as additives in the preparation of various antistatic composites, as contact and current-carrying elements in control and measurement equipment.

References

Yu, C., Zhang, W., Guo, S., Hu, B., Zheng, Z., Ye, J., Zhu, J. (2019). A safe and efficient liquid-solid synthesis for copper azide films with excellent electrostatic stability. Nano energy, – 66. – 104135 p.

Sun, X., Mo, X., Liu, L., Sun, H., & Pan, C. (2019). Voltage-driven room-temperature resistance and magnetization switching in ceramic TiO_2/PAA nanoporous composite films. ACS appl. mater&inter., – 11(24). – P. 21661–21667.

Zhang, K., Cao, S., Li, C., Qi, J., Jiang, L., Zhang, J., & Zhu, X. (2019). Rapid growth of TiO_2 nanotubes under the compact oxide layer: Evidence against the digging manner of dissolution reaction. Electrochem. Comm, – 103. – P. 88–93.

Lee, W., & Park, S. J. (2014). Porous anodic aluminum oxide: anodization and templated synthesis of functional nanostructures. Chem. Rev., – 114(15). – 7487 p.

Cheng, Y., Peng, Z., Wu, X., Cao, J., Skeldon, P., & Thompson, G. E. (2015). A comparison of plasma electrolytic oxidation of Ti-6Al-4V and Zircaloy-2 alloys in a silicate-hexametaphosphate electrolyte. Electroch. Acta, – 165, – 301 p.

Li, Z., Li, Y., Li, S., Wu, J., Hu, X., Ling, Z., & Jin, L. (2018). A modified quantitative method for regularity evaluation of porous AAO and related intrinsic mechanisms. Journal of The Electrochemical Society, – 165(5). – E214.

Feng, C., Zhang, Z., Li, J., Qu, Y., Xing, D., Gao, X., ... & Sun, R. (2019). A bioinspired, highly transparent surface with dry style antifogging, antifrosting, antifouling, and moisture self-cleaning properties. Macromolecular rapid communications, – 40(6). – 1800708 p.

Wang, K., Liu, G., Hoivik, N., Johannessen, E., & Jakobsen, H. (2014). Electrochemical engineering of hollow nanoarchitectures: pulse/step anodization (Si, Al, Ti) and their applications. Chem. Soc. Rev., – 43(5). – 1476 p.

Lee, K., Mazare, A., & Schmuki, P. (2014). One-dimensional titanium dioxide nanomaterials: nanotubes. Chemical reviews, – 114(19). – P. 9385–9454.

Zhang, Y., Cheng, W., Du, F., Zhang, S., Ma, W., Li, D., Zhu, X. (2015). Quantitative relationship between nanotube length and anodizing current during constant current anodization. Electrochimica Acta, – 180. – P. 147–154.

Cui, H., Chen, Y., Lu, S., Zhang, S., Zhu, X., & Song, Y. (2017). TiO_2 nanotube arrays treated with $(NH_4)_2TiF_6$ dilute solution for better supercapacitive performances. Electrochimica Acta, – 253. – P. 455–462.

Li, W., Zhang, W., Li, T., Wei, A., Liu, Y., & Wang, H. (2019). An Important Factor Affecting the Supercapacitive Properties of Hydrogenated TiO_2 Nanotube Arrays: Crystal Structure. Nanoscale Research Letters, – 14. – P. 1–14.

Sopha, H., Jäger, A., Knotek, P., Tesař, K., Jarosova, M., & Macak, J. M. (2016). Self-organized anodic TiO_2 nanotube layers: Influence of the Ti substrate on nanotube growth and dimensions. Electrochimica Acta, – 190. – 744 p.

Zhang, J., Li, Y., Zhang, Y., Qian, X., Niu, R., Hu, R., Zhu, J. (2018). The enhanced adhesion between overlong TiNxOy/MnO_2 nanoarrays and Ti substrate: Towards flexible supercapacitors with high energy density and long service life. Nano Energy, – 43. – P. 91–102.

Zhao, S., Chen, Y., Zhao, Z., Jiang, L., Zhang, C., Kong, J., & Zhu, X. (2018). Enhanced capacitance of TiO_2 nanotubes topped with nanograss by H_3PO_4 soaking and hydrogenation doping. Electrochimica Acta, – 266. – P. 233–241.

Wang, L., Wei, Z., Sun, Z., Zhu, L., Gao, Y., Chen, Z., Chen, W. (2024). Carbon-based double-metal-site catalysts: advances in synthesis and energy applications. J. Mater. Chem A, – 12(20). – P. 11749–11770.

submitted 11.11.2024;
accepted for publication 25.11.2024
published 30.01.2025

Contact: todjiyev88@mail.ru